Fabrication, Patterning, and Optical Properties of Nanocrystalline YVO_4:A (A = Eu^{3+}, Dy^{3+}, Sm^{3+}, Er^{3+}) Phosphor Films via Sol−Gel Soft Lithography

M. Yu,[†] J. Lin,*[,†] Z. Wang,[‡] J. Fu,[‡] S. Wang,[†] H. J. Zhang,[†] and Y. C. Han*[,‡]

Key Laboratory of Rare Earth Chemistry and Physics, and State Key Laboratory of Polymer Physics and Chemistry, Changchun Institute of Applied Chemistry, Chinese Academy of Sciences, Changchun 130022, People's Republic of China

Received November 28, 2001. Revised Manuscript Received February 21, 2002

Nanocrystalline YVO_4:A (A = Eu^{3+}, Dy^{3+}, Sm^{3+}, Er^{3+}) phosphor films and their patterning were fabricated by a Pechini sol−gel process combined with soft lithography. X-ray diffraction (XRD), Fourier transform infrared spectroscopy (FT-IR), thermogravimetric and differential thermal analysis (TG-DTA), atomic force microscopy (AFM) and optical microscopy, UV/vis transmission and absorption spectra, photoluminescence (PL) spectra, and lifetimes were used to characterize the resulting films. The results of XRD indicated that the films began to crystallize at 400 °C and the crystallinity increased with the increase of annealing temperatures. Transparent nonpatterned phosphor films were uniform and crack-free, which mainly consisted of grains with an average size of 90 nm. Patterned gel and crystalline phosphor film bands with different widths (5−60 μm) were obtained. Significant shrinkage and a few defects were observed in the patterned films during the heat treatment process. The doped rare earth ions (A) showed their characteristic emission in crystalline YVO_4 phosphor films because of an efficient energy transfer from vanadate groups to them. The Sm^{3+} and Er^{3+} ions also showed upconversion luminescence in a YVO_4 film host. Both the lifetimes and PL intensity of the rare earth ions increased with increasing annealing temperature from 400 to 800 °C, and the optimum concentration for Eu^{3+} was determined to be 7 mol % and those for Dy^{3+}, Sm^{3+}, and Er^{3+} were 2 mol % of Y^{3+} in YVO_4 films, respectively.

I. Introduction

In recent years, the interest in phosphor thin films have been growing because of their potential application in high-resolution devices such as cathode ray tubes (CRTs), flat panel display devices, and field emission displays (FEDs).[1] Displays with thin film phosphors have higher contrast and resolution and superior thermal conductivity as well as a high degree of uniformity and better adhesion.[2] Thin phosphor films have been prepared by a variety of deposition techniques, such as chemical vapor deposition (CVD),[3] spray pyrolysis,[4] and pulsed laser deposition.[5] Generally, these techniques need expensive and complicated equipment setups. Therefore, a simple and economical method for making high-quality thin film phosphors is desirable. The solution-based sol−gel method is one of the most important techniques for the synthesis of various functional coating films because it possesses a number of advantages over conventional film formation techniques, such as low processing temperature, easy coating of large surfaces, and possible formation of porous films and homogeneous multicomponent oxide films.[6] In fact, some efforts have been made to develop various kinds of luminescent films via the sol−gel method in the past decade. Representative examples are $Y_3Al_5O_{12}$:Tb[1] and Y_2SiO_5:Tb[2] films for cathodoluminescence, $Y_3Al_5O_{12}$:Eu[7] films for field emission displays, and Y_2O_3:Eu[8] and Zn_2SiO_4:Mn[9] films for photoluminescence. In most of the above cases, the sol−gel precursors used are metal alkoxides and/or organometallic compounds, which suffer from high cost, toxicity, and difficulty in controlling the experimental processes. An alternative approach to form nanocrystalline thin film is the Pechini-type sol−gel process, which mainly employs the inorganic salts as precursors, citric acid as a chelate ligand, and poly(ethylene glycol) (PEG) as a cross-linking agent.[10]

On the other hand, the patterning technologies of phosphor screens have a great effect on the resolution of flat panel display devices.[11] For instance, pitches of

* To whom correspondence should be addressed. E-mail: jlin@ns.ciac.jl.cn.
[†] Key Laboratory of Rare Earth Chemistry and Physics.
[‡] State Key Laboratory of Polymer Physics and Chemistry.

(1) Choe, J. Y.; Ravichandran, D.; Biomquist, S. M.; Morton, D. C.; Kirchner, K. W.; Ervin, M. H.; Lee, U. *Appl. Phys. Lett.* **2001**, *78*, 3800.
(2) Rabinovich, E. M.; Shmulovich, J.; Fratello, V. J.; Kopyov, N. J. *Am. Ceram. Soc. Bull.* **1987**, *6*, 1505.
(3) Bai, G. R.; Zhang, H.; Foster, C. M. *Thin Solid Films* **1998**, *321*, 115.
(4) Hao, J.; Studenikin, S. A.; Cocivera, M. *J. Lumin.* **2001**, *93*, 313.
(5) Korzenski, M. B.; Lecoeur, Ph.; Mercey, B.; Raveau, B. *Chem. Mater.* **2001**, *13*, 545.
(6) Sakka, S. *Struct. Bonding* **1996**, *85*, 1.
(7) Ravichandran, D.; Roy, R.; Chakhovskoi, A. G.; Hunt, C. E.; White, W. B.; Erdei, S. *J. Lumin.* **1997**, *71*, 291.
(8) Rao, R. P. *Solid State Commun.* **1996**, *99*, 439.
(9) Lin, J.; Saenger, D. U.; Mennig, M.; Baerner, K. *Thin Solid Films* **2000**, *360*, 39.
(10) Pechini, M. P. U.S. Patent 3,330,697, 1967.

10.1021/cm011663y CCC: $22.00
Published on Web 04/04/2002

phosphor lines for a supervideo graphics adapter with 800 × 600 lines, a video graphics adapter with 640 × 480 lines, and a quarter video graphics adapter with 320 × 240 lines in 6-in. color displays are defined as 50.8, 63.5, and 127 μm, respectively. Considering the spacer and blank matrix areas, the corresponding phosphor line width should be below 30, 40, and 70 μm, respectively. Therefore, a precise screening process for high resolution is desirable. The current used patterning techniques for a phosphor screen include electrophoretic deposition,[12] screen printing,[13] etc. based on photolithography, which needs complicated and expensive photolithographic and etching equipment. Recently, however, much attention has been paid to non-photolithographic patterning techniques collectively known as soft lithography, which have the potential of becoming versatile and low-cost methods for creating micrometer- and submicrometer-size structures.[14] So far, many reports describing the use of soft lithography to fabricate patterned structures can be found in the literature.[15−17] However, most of these experiments focused on relatively simple systems of single oxides or polymer materials.

So far, neither the work of phosphor films via the Pechini-type sol−gel process nor their direct patterning via soft lithography have been reported in the literature. Yttrium vanadate (YVO_4) has been shown to be a useful host lattice for rare earth ions to produce phosphors emitting a variety of colors.[18−20] Eu^{3+}-activated YVO_4 is an important commercial red ($^5D_0-{}^7F_2$ of Eu^{3+} at 618 nm) phosphor used in color television, the cathode ray tube, and the high-pressure mercury lamp, which was first introduced by Levine and Palilla.[21] Dy^{3+}-activated YVO_4 is a potential white phosphor because of the yellow ($^4F_{9/2}-{}^6H_{13/2}$) and blue ($^4F_{9/2}-{}^6H_{15/2}$) emissions of Dy^{3+}.[22] YVO_4 and Nd^{3+}-doped YVO_4 thin films have been fabricated by CVD and alkoxy sol−gel[23,24] and pulsed laser deposition,[25] respectively. In this paper, we report a Pechini sol−gel synthesis of the nanocrystalline YVO_4:A (A = Eu^{3+}, Dy^{3+}, Sm^{3+}, Er^{3+}) thin phosphor films and their patterning via soft lithography (micromolding in capillaries) as well as their photoluminescence properties.

II. Experimental Section

Preparation of the Films. Nonpatterned thin films of YVO_4:A (A = Eu^{3+}, Dy^{3+}, Sm^{3+}, Er^{3+}) phosphor samples were prepared by a Pechini sol−gel and dip-coating method.[10] The doping concentration of the rare earth ion (A) was 0.1−12 mol % that of Y^{3+} in the YVO_4 host. The stoichiometric amounts of Y_2O_3 (99.99%), Eu_2O_3 (99.99%), Dy_2O_3 (99.95%), Sm_2O_3 (99.9%), Er_2O_3 (99.9%), and NH_4VO_3 (99%, A.R.) were dissolved in dilute HNO_3 (A.R.) and then were mixed with a water−ethanol (v/v = 1:7) solution containing citric acid (A.R.) as a chelating agent for the metal ions. The molar ratio of metal ions to citric acid was 1:2. A certain amount of poly(ethylene glycol) (PEG, molecular weight = 10000, A.R.) was added as a cross-linking agent. The solution was stirred for 1 h to form a sol and then dip-coated on thoroughly cleaned silica glass substrates at a speed of 0.2 cm/s. The coatings were dried immediately at 100 °C for 1 h. Then, the dried films were annealed to the desired temperature (300−800 °C) with a heating rate of 1 °C/min and held there for 2 h in air.

Patterning of the Films. The patterning of the phosphor films was carried out by soft lithography as described previously.[14−16] First, poly(dimethylsiloxane) (PDMS) stamp modes were fabricated by casting PDMS on masters having desired patterns. In a typical experimental procedure, we placed a master in a glass Petri dish and poured a 10:1 (v/v) mixture of SYLGARD silicone elastomer 184 and its curing agent (Dow Corning Corp.) over the master. The elastomer was degassed for ≈30 min at room temperature, cured at 65 °C for about 4 h, and then peeled gently from the master. In this way the PDMS modes with different channel widths (5−60 μm) were obtained.

The PDMS modes were placed in conformal contact with thoroughly cleaned silicon wafer substrates. The channels of the mode thus formed capillaries with the silicon wafer substrate. The above sol for dip coating was then dropped at the open end with a transfer pipet. The capillary force made the sol flow into the mold. Then, the modes and substrates were dried at 100 °C overnight. After careful removal of the modes, the resulted patterned gel films were heated to 700 °C with a heating rate of 1 °C/min and held there for 2 h in air.

Characterization. The X-ray diffraction (XRD) of the film and powder samples was examined on a Rigaku-Dmax 2500 diffractometer using Cu Kα radiation (λ = 0.15405 nm). FT-IR spectra were measured with Perkin-Elmer 580B infrared spectrophotometer with the KBr pellet technique. A TA Instruments thermal analyzer was used to record TGA-DTA curves of the gel powders with a heating rate of 10 °C/min. The thickness of the transparent nonpatterned crystalline films was measured on a AUEL-III automatic laser ellipsometer. The morphology of the crystalline film sample was inspected using an atomic force microscope (AFM, Seiko) with tapping mode. Patterned film pictures were taken on an Lcica DMLP optical microscope. The UV/vis absorption and transmission spectra were measured on a TU-1901 spectrophotometer. The excitation and emission spectra were taken on a SPEX FL-2T2 spectrofluorimeter equipped with a 450-W xenon lamp as the excitation source. Luminescence lifetimes were measured with a SPEX 1934D phosphorimeter using a 7-W-pulse xenon lamp as the excitation source with a pulse width of 3 μs. All the measurements were performed at room temperature (RT).

III. Results and Discussion

Formation Process and Structures of the Phosphor Films. *XRD.* Figure 1 shows the XRD profiles of the films annealed from 300 to 700 °C (a−d) and that of the powder annealed at 500 °C (e) as a comparison. For the film annealed at 300 °C, no diffraction peak is observed except for the broad band at 2 Å = 22.02°, which is ascribed to a quartz glass substrate. This indicates that the film remains amorphous below this

(11) Jang, J. E.; Gwak, J.-H.; Jin, Y. W.; Lee, S. J.; Park, S. H.; Jung, J. E.; Lee, N. S.; Kim, J. M. *J. Vac. Sci. Technol. B* **2000**, *18*, 1106.
(12) Sluzky, E.; Hesse, K. *J. Electrochem. Soc.* **1989**, *126*, 2742.
(13) Holmes, P. J.; Loasby, R. G. *Handbook of Thick Film Technology*; Electrochemical Publications: Ayr, 1976; p 50.
(14) Xia, Y.; Whiteside, G. M. *Annu. Rev. Mater. Sci.* **1998**, *28*, 153.
(15) Hu, J.; Beck, R. G.; Whiteside, R. M. *Adv. Mater.* **1998**, *10*, 574.
(16) Seraji, S.; Wu, Y.; Jewell-Larson, N. E.; Forbess, M. J.; Limmer, S. J.; Chou, T. P.; Cao, G. *Adv. Mater.* **2000**, *12*, 1421.
(17) Jeon, N. L.; Hu, J.; Whiteside, G. M.; Erhardt, M. K.; Nuzzo, R. G. *Adv. Mater.* **1998**, *10*, 1466.
(18) Riwotzki, K.; Haase, M. *J. Phys. Chem. B* **1998**, *102*, 10129.
(19) Huignard, A.; Gacoin, T.; Boilot, J. P. *Chem. Mater.* **2000**, *12*, 1090.
(20) Hsu, C.; Powell, R. C. *J. Lumin.* **1975**, *10*, 273.
(21) Levine, A. K.; Palilla, F. C. *Appl. Phys. Lett.* **1964**, *5*, 118.
(22) Sommerdijk, J. L.; Bril, A.; Hoex-Stril, F. M. J. H. *Philips Res. Rep.* **1977**, *32*, 149.
(23) Yamaguchi, O.; Mukaida, Y.; Shigeta, H.; Takemura, H.; Yamashita, M. *J. Electrochem. Soc.* **1989**, *136*, 1557.
(24) Hirano, S.; Yogo, T.; Kikuta, K.; Sakamoto, W.; Koganei, H. *J. Am. Ceram. Soc.* **1996**, *79*, 3041.
(25) Korzenski, M. B.; Lecoeur, Ph.; Mercey, B.; Raveau, B. *Chem. Mater.* **2001**, *13*, 545.

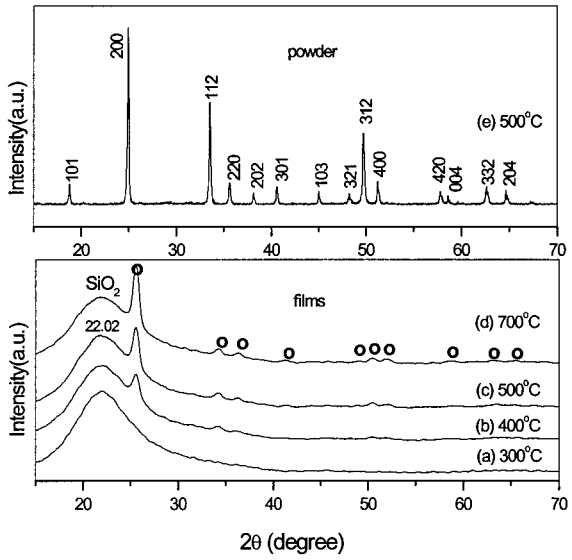

Figure 1. X-ray diffraction patterns for YVO_4:0.04Eu films and powder annealed at different temperatures.

temperature. For the sample fired at 400 °C, two weak and broad peaks at 2 Å = 24.92° and 33.48° due to the (200) and (112) reflections of YVO_4 are present, suggesting the starting of crystallization at this stage. After annealing at 500 and 700 °C, other diffraction peaks belonging to the crystalline YVO_4 have been observed clearly (JCPDS Card 17-341). All the diffraction peaks due to YVO_4 can be seen more obviously in the XRD pattern of the powder annealed at 500 °C, as shown in Figure 1e. No second phase is detected. Note that the diffraction peaks of the YVO_4 film are a little broader and have a higher degree of shift than the counterparts of YVO_4 powder, indicating that the size of the crystalline grains in the film is smaller than that in the powder. In fact, the calculated crystal cell parameters (a = 0.702 nm, c = 0.619 nm, V = 0.305 nm^3) for crystalline YVO_4 in the film are a little smaller than those (a = 0.725 nm, c = 0.629 nm, V = 0.330 nm^3) in the powder. This may be caused by slightly different crystallization behaviors between the film and powder samples. Furthermore, it can be seen clearly that the YVO_4 film crystallized with (200) preferred orientation on the silica glass substrate, as observed previously.[24]

FT-IR. The FT-IR spectra of the gel powders annealed from 100 to 700 °C are shown in Figure 2. For the sample dried at 100 °C, the FT-IR spectrum shows the absorption bands of the H_2O and −OH group (3500, 3200, and 3075 cm^{-1}), $-CH_2$ group (2914 and 2878 cm^{-1}), NO_3^- group (1646 cm^{-1}), carbonates COO^- (1440 and 1365 cm^{-1}), and VO_3^- group (942 and 835 cm^{-1}), all of which arise from the starting materials such as citric acid, PEG, $Y(NO_3)_3$, and NH_4VO_3. The absorption intensity of these bands decreases with increasing sintering temperature because of the pyrolysis of the organic species. Although the organic impurities (COO^-) still can be observed in the FT-IR spectrum of the film sample annealed at 400 °C, a strong absorption band at 805 cm^{-1} and a weak band at 472 cm^{-1} have appeared, which are attributed to the absorption of V−O (from the VO_4^{3-} group) and Y−O bonds, respectively.[24] This suggests that yttrium vanadate (YVO_4) has formed at this temperature (400 °C), agreeing well with the results of XRD. Further heat treatment results in a higher energy shift for the absorption of the V−O bond (811 cm^{-1} for 500 °C and 823 cm^{-1} for 600 and 700 °C) and the disappearance for the absorption of organic impurities, indicating that the V−O bond becomes stronger because of the improvement of the crystallinity with increasing annealing temperature.

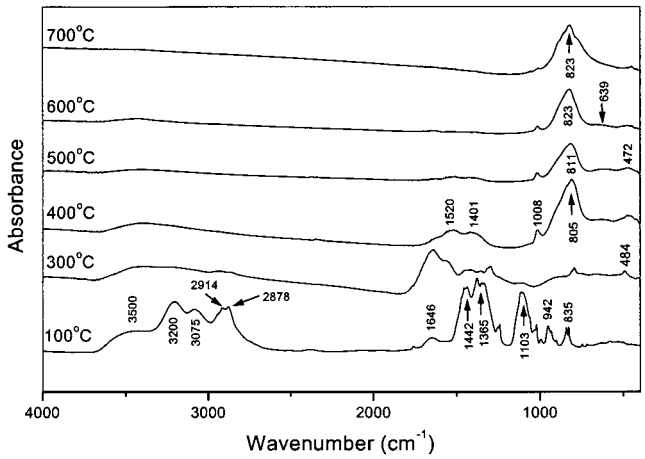

Figure 2. FT-IR spectra of YVO_4:0.04Eu precursor powders annealed at different temperatures.

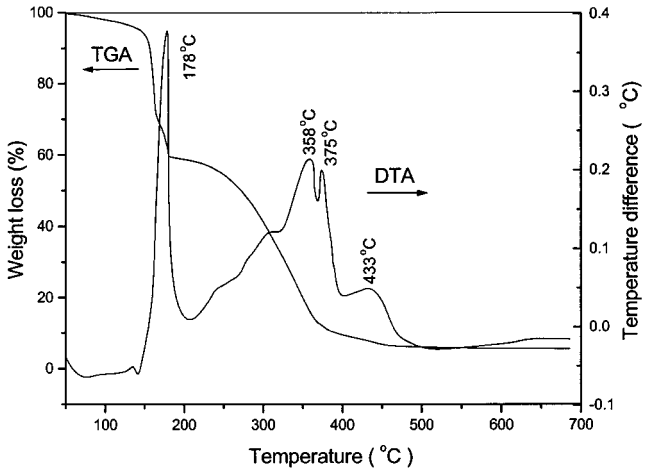

Figure 3. TG-DTA curves of YVO_4:0.04Eu gel powder.

TG-DTA. The precursor solution was evaporated to yield powder, which was analyzed by TG-DTA. Figure 3 shows the TG-DTA curves of the powder heat-treated in air. The TG curve shows four stages of weight loss. The first weight loss (5%) step is observed between 50 and 145 °C because of the evaporation of water and organic solvents. The second weight loss (38%) is from 145 to 200 °C, accompanied by a strong exothermic peak at 178 °C in the DT curve because of the burnout of excess citric acid and ethanol. The third weight loss step (50%) is noticed between 250 and 380 °C accompanied by two strong exothermic peaks at 358 and 375 °C in the DT curve. This is caused by further combustion of the organic groups in PEG, citric acid, the polyester (formed by the reaction between PEG and citric acid), and the citrates. The final weight loss (5%) is from 380 to 500 °C accompanied with an exothermic peak at 433 °C in the DTA curve because of the crystallization of the YVO_4 phase, basically agreeing with the results of XRD and FT-IR.

AFM and Optical Micrographs. The 700 °C annealed transparent film (nonpatterned, dip coating) had a

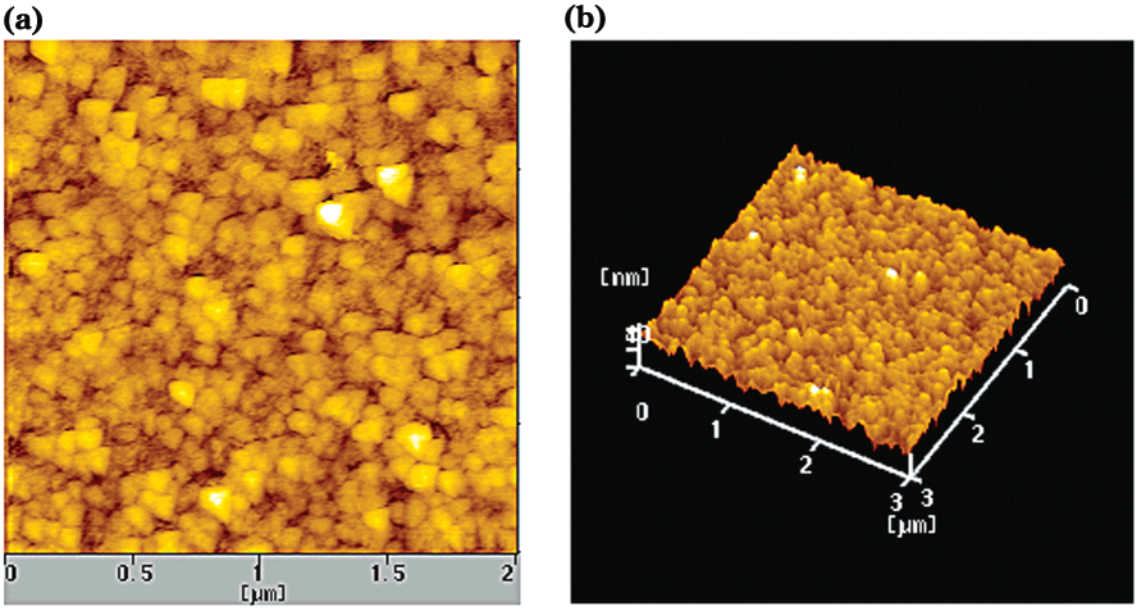

Figure 4. AFM images of the transparent YVO_4:0.04Eu film annealed at 700 °C: (a) planar image; (b) stereo image.

thickness of 150 nm (measured on a AUEL-III automatic laser ellipsometer). The morphology of the crystalline film sample was inspected using an atomic force microscope (AFM). The AFM image of the transparent film annealed at 700 °C is shown in Figure 4. It is known from planar image that the film, which is uniform and crack-free, mainly consists of closely packed fine particles with an average grain size of 90 nm (Figure 4a). The film surface is well-crystallized and very smooth with a RMS roughness of 4.55 nm (stereo image in Figure 4b).

The patterning of the phosphor films was performed in the Eu^{3+}-doped YVO_4 system. Figure 5 shows optical micrographs for the patterned structures of YVO_4:0.04Eu gel (a, b, 100 °C dried) and crystalline (c, d, annealed at 700 °C) films. The dark and white regions correspond to the films' bands and spaces, respectively. Defect-free gel film bands having widths of 53 μm (with a space of 37 μm) and 24 μm (with a space of 12 μm) can be seen clearly in Figure 5a,b, respectively. From Figure 5a one can observe clearly how the film bands were produced. At the open end the sol flowed into the channels between the substrate and the mode, forming patterned gel film bands after drying. Some small pieces of gel can still be found between two gel film bands at the open end of the mode because of a loose contact of the substrate with the mode in these regions. However, in other parts the channels were fully filled with the sols, resulting in homogeneous and smooth gel film bands. After firing, the gel film bands began to crystallize, accompanied by the formation of a few defects and shrinkage for the film bands. This can be seen clearly in Figure 5c and its inset (enlarged film bands). The actual width of the crystalline film band derived from the mode with a 21-μm-wide channel is only about 14 μm; that is, a 30−40% shrinkage in width has occurred after crystallization. The edge lines between the film band and space caused by the shrinkage can also be seen clearly. This is not surprising, for it is well-known that the evaporation and pyrolysis of organic compounds in a gel is accompanied by significant shrinkage.[26] The TGA curve of the dried gel showed a weight loss of more than 90% from 100 to 700 °C (Figure 3), which made the shrinkage in the crystalline film bands more understandable. Additionally, owing to the shrinkage, the surface of the crystalline film bands is not as smooth as that of gel film bands. Even narrow crystalline film bands with 7-μm width and space have been obtained, and no obvious defects can be detected, as shown in Figure 5d. The crystalline patterned YVO_4:Eu films show a strong red emission under the irradiation of UV light, and the emission intensity seems to increase with decreasing width of film bands.

Optical Properties. The patterned and nonpatterned phosphor films show similar optical properties. So all the characterizations for the optical properties were performed on the nonpatterned films because of their relatively easy availability.

Spectral Properties of YVO_4:A (A = Eu, Dy, Sm, Er) Films. Figure 6 shows the UV/vis transmission spectrum of YVO_4:0.04Eu film annealed at 700 °C. There is no absorption between 350 and 800 nm, indicating the high transparency of the film in the visible region. Figure 7 displays the absorption spectra for YVO_4 (a) and YVO_4:0.02Dy (c), PL excitation (b) and emission (d) spectra for YVO_4:0.02Dy, and a PL emission spectrum (e) for YVO_4:0.04Eu. A strong absorption band with maximum values at 276 nm is observed for both YVO_4 and YVO_4:0.02Dy (and YVO_4:0.04Eu, Figure 6) films, which agrees well with the absorption spectra of a colloid solution of nanocrystalline YVO_4:Eu.[18,19] Obviously, this band is ascribed to a charge transfer from the oxygen ligands to the central vanadium atom inside the VO_4^{3-} ion. From the viewpoint of molecular orbital theory, it corresponds to transitions from the $^1A_2(^1T_1)$ ground state to $^1A_1(^1E)$ and $^1E(^1T_2)$ excited states of the VO_4^{3-} ion.[20] The 700 °C annealed YVO_4:0.02Dy transparent film shows a strong yellow emission (close to white) under

(26) Brinker, C. J.; Scherer, G. W. *Sol−Gel Sciences*; Academic Press: San Diego, CA, 1990.

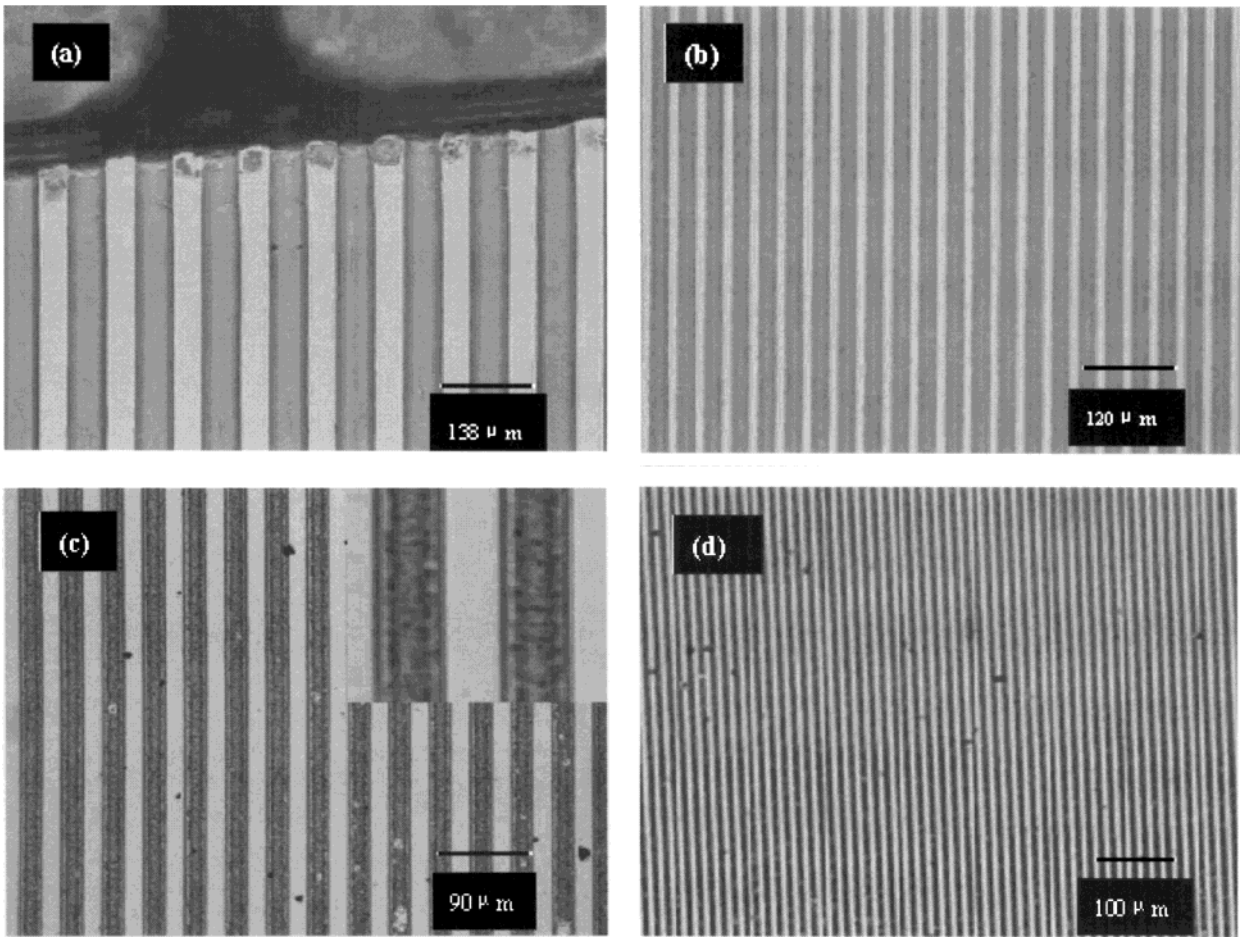

Figure 5. Optical micrographs of the patterned gel (a, b, dried at 100 °C) and crystalline (c, d, annealed at 700 °C) YVO_4:0.04Eu phosphor films.

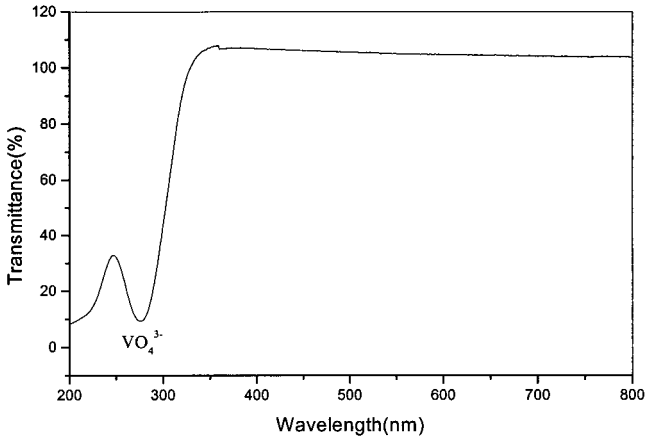

Figure 6. UV/vis transmission spectrum of YVO_4:0.04Eu film annealed at 700 °C.

UV excitation. The excitation spectrum (Figure 7b) consists of an intense band with a maximum at 276 nm because of VO_4^{3-} absorption, which agrees well the absorption spectra (Figure 7a,c). Excitation into the vanadate group at 276 nm yields the emission spectrum (Figure 6d), which contains exclusively the characteristic transition lines of Dy^{3+}, that is, $^4F_{9/2}-^6H_{15/2}$ (482 nm, blue), $^4F_{9/2}-^6H_{13/2}$ (573 nm, yellow), and $^4F_{9/2}-^6H_{11/2}$ (664 nm, red). No emission from VO_4^{3-} is detected, indicating an efficient energy transfer from VO_4^{3-} to Dy^{3+} in the phosphor films. The same situation holds for that of crystalline YVO_4:0.04Eu film, which shows a strong red emission under UV excitation. The excitation spectrum monitored with 618-nm emission of Eu^{3+} ($^5D_0-^7F_2$) is similar to that of YVO_4:0.02Dy film (Figure 7b). In this emission spectrum (Figure 7e), not only the characteristic transition lines from the lowest excited $^5D_0$ level of Eu^{3+} are observed but also those from higher energy levels ($^5D_1$,$^5D_2$, and $^5D_3$) of Eu^{3+} are detected with a very weak intensity. The locations of the emission lines of Eu^{3+} and their assignments are indicated in the figure. Obviously, the strong emission of Eu^{3+} is also due to an efficient energy transfer from the VO_4^{3-} group to Eu^{3+} in YVO_4:0.04Eu films.

Both Eu^{3+} $^5D_0-^7F_2$ and Dy^{3+} $^4F_{9/2}-^6H_{13/2}$ emissions belong to hypersensitive transitions with $\Delta J = 2$, which are strongly influenced by outside surroundings. When the Eu^{3+} or Dy^{3+} is located at a low-symmetry local site (without an inversion center), these two emission transitions are often dominated in their emission spectra. This is actually the case for Eu^{3+} and Dy^{3+} in the YVO_4 film host lattices. The crystalline YVO_4 adopts the tetragonal structure with a space group of I_1/amd, which is composed of YO_8 dodecahedra (the point symmetry of Y^{3+} is D_{2d}, without an inversion center) and VO_4 tetrahedra (T_d).[20] The Eu^{3+} and Dy^{3+} ions occupy the Y^{3+} sites in YVO_4 films, resulting in the hypersensitive transitions ($^5D_0-^7F_2$ of Eu^{3+} and $^4F_{9/2}-^6H_{13/2}$ of Dy^{3+}) being the most prominent group in their emission spectra, respectively. In addition, the crystal field splitting of Eu^{3+} $^5D_0-^7F_{1,2,4}$ transitions can be seen clearly, indicating that the film is well-crystallized. The pres-

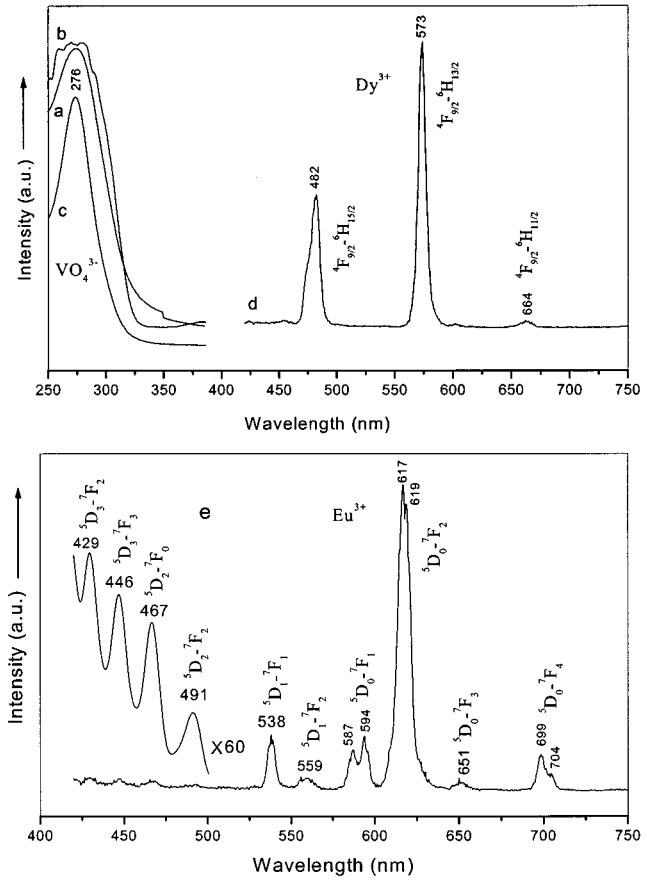

Figure 7. Absorption spectrum for YVO_4 film (a), excitation (b, $\lambda_{em} = 573$ nm), absorption (c), and emission (d, $\lambda_{ex} = 276$ nm) spectra for YVO_4:0.02Dy film and emission spectrum for YVO_4: 0.04Eu film (e, $\lambda_{ex} = 276$ nm).

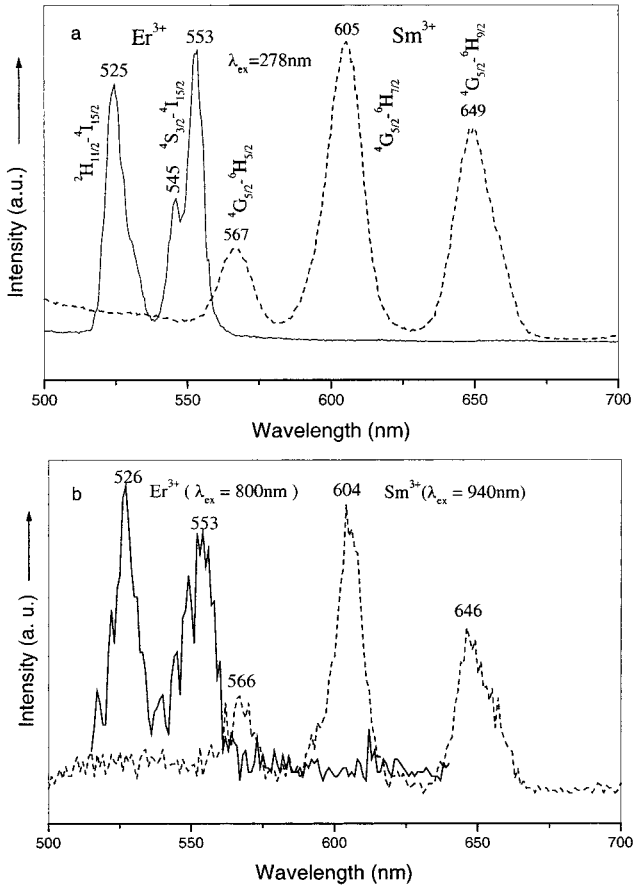

Figure 8. Downconversion (a) and upconversion (b) emission spectra of YVO_4:0.02Sm and YVO_4:0.02Er films.

ence of emission lines from higher excited states of Eu^{3+} ($^5D_1$, $^5D_2$, and $^5D_3$) is attributed to the low vibration energy of VO_4^{3-} groups (823 cm^{-1}). The multiphonon relaxation by VO_4^{3-} is not able to bridge the gaps between the higher energy levels ($^5D_1$, $^5D_2$, and $^5D_3$) and the $^5D_0$ level of Eu^{3+} completely, resulting in weak emissions from these levels. In silicate and borates where $\nu_{max} = 1000-1200$ cm^{-1}, such emissions cannot be detected.[27]

The excitation and absorption spectra for crystalline YVO_4:Sm and YVO_4:Er films are very similar to those in Figure 7a–c; that is, only a strong band with a maximum at 276 nm due to the VO_4^{3-} group has been observed. Excitation into the vanadate group at 276 nm yields the characteristic red-orange emission of Sm^{3+} at 567 nm ($^4G_{5/2}-^6H_{5/2}$), 605 nm ($^4G_{5/2}-^6H_{7/2}$), and 649 nm ($^4G_{5/2}-^6H_{9/2}$) and green emission of Er^{3+} at 525 nm ($^2H_{11/2}-^4I_{15/2}$), 545 nm, and 553 nm ($^4S_{3/2}-^4I_{15/2}$), respectively, as shown in Figure 8a. This indicates that, similarly to the situations for Eu^{3+} and Dy^{3+}, an efficient energy transfer also occurs from VO_4^{3-} to Sm^{3+} and Er^{3+} in YVO_4 film. Furthermore, the upconverted luminescence phenomena of Er^{3+} and Sm^{3+} have been observed in YVO_4 film. Figure 8b shows the upconverted emission spectrum of Er^{3+} excited with 800 nm and that of Sm^{3+} excited with 940 nm. The characteristic green emission (520–560 nm) of Er^{3+} and red emission (560–670 nm) of Sm^{3+} have been clearly observed in these emission spectra.

To our knowledge, the upconversion for Sm^{3+} has only been reported in low-phonon hosts such as $LaBr_3$[28] and nanocrystalline CaS:Sm^{3+}.[29] It is the first observation for the upconversion phenomenon of Sm^{3+} in a YVO_4 (film) host. Under infrared light 940-nm excitation, the $^4G_{5/2}$ excited state of Sm^{3+} can be populated by two possible approaches: the excited-state absorption (EAS) and energy-transfer (ET) processes, as shown in Figure 9. For the ESA process, after a first excitation to the $^6F_{11/2}$ level, a second photon is absorbed by the same ion, exciting it to $^4I_{11/2}$ state, that is, $^6H_{5/2} \rightarrow {}^6F_{11/2} \rightarrow {}^4I_{11/2}$; for the ET process, one of the two coupled Sm^{3+}, simultaneously excited through the ground-state absorption by infrared photons to the $^6F_{11/2}$ state, transfer its energy to the neighboring ion, leaving it in the higher excited states ($^4I_{11/2}$ etc.). Both approaches excite the Sm^{3+} to the $^4I_{11/2}$ (or $^4G_{7/2}$ and $^4F_{3/2}$) state, from which the $^4G_{5/2}$ energy level is populated by multiphonon deexcitation. As a result, anti-Stokes emissions from the $^4G_{5/2}$ excited state to the ground states ($^6H_{5/2}$, $^6H_{7/2}$, and $^6H_{9/2}$) are observed. In view of the short lifetime (on the order of 10 ns) of the $^6F_{11/2}$ level of Sm^{3+}, ESA transitions from this level are not likely to occur.[30] So

(27) Blasse, G.; Grabmaier, B. C. *Luminescent Materials*; Springer-Verlag: Berlin, 1994; Chapter 4.

(28) Areva, S.; Holsa, J.; Lamminmaki, R.-J.; Rahiala, H.; Deren, P.; Strek, W. In *Third International Winter Workshop RES'99*, Szklarska Poreba, Poland, 27 April; 1999; p 67.

(29) Gong, X.; Chen, W. J.; Wu, P. F.; Chan, W. K. *Appl. Phys. Lett.* **1998**, *73*, 2875.

(30) Reisfeld, R.; Jorgensen, C. K. *Laser and Excited States of Rare-earths*; Springer: Heidelbeerg, 1997.

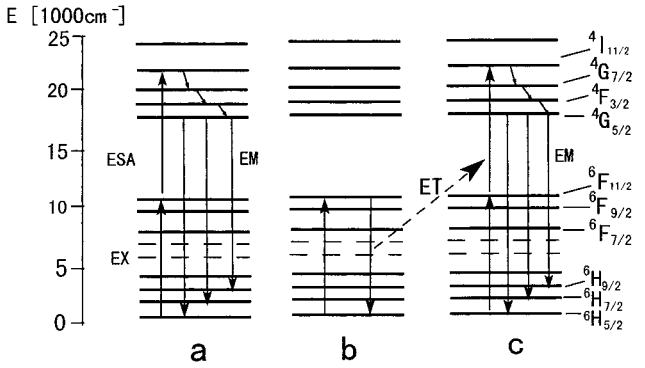

Figure 9. Schematic diagram of ESA (a) and ET (b) + (c) approaches for the upconversion of Sm^{3+} under 940-nm excitation.

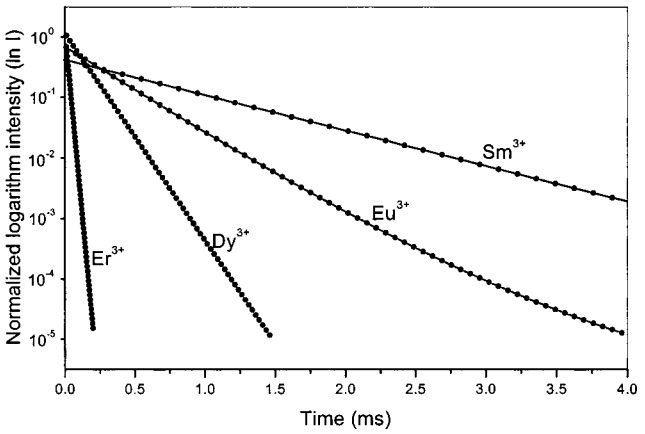

Figure 10. Decay curves of Eu^{3+}, Dy^{3+}, Sm^{3+}, and Er^{3+} luminescence in crystalline YVO_4 films annealed at 700 °C.

the most probable mechanism for the upconversion luminescence of Sm^{3+} in the YVO_4 film host is energy transfer between two Sm^{3+} ions.

Er^{3+} is a well-known rare earth ion having upconversion luminescence properties,[27] and the green upconverted emission of Er^{3+} in YVO_4 crystals has been reported, whose mechanism have been well-established.[31,32] Similar to Sm^{3+}, under 800-nm excitation, both the ESA and ET processes can excite the Er^{3+} to the $^2G_{9/2}$ state, from which $^4S_{3/2}$ and $^2H_{11/2}$ states are populated via multiphonon de-excitation. A detailed study by S. Golab et al.[31] indicated that the ESA processes from $^4I_{9/2}$ and $^4I_{11/2}$ levels of Er^{3+} in YVO_4 govern the upconversion phenomenon under excitation around 800 nm.

Temperature Effects. The lifetimes and emission intensity of the rare earth ions (Eu^{3+}, Dy^{3+}, Sm^{3+}, and Er^{3+}) have been studied as a function of annealing temperature in YVO_4 films. The decay curves for the luminescence of the rare earth ions in the YVO_4 films annealed at 700 °C are shown in Figure 10. In general, all these curves can be well-fitted into a single-exponential function as $I = I_0 + C\exp[-(t - t_0)/\tau]$ (C is constant, τ is the 1/e lifetime of the rare earth ion), confirmed by the straight line character of ln(I) versus time in Figure 10. This indicates that the coordination environment of the rare earth ions is homogeneous in YVO_4 films. The lifetimes (τ) of excited states for Eu^{3+} ($^5D_0$), Dy^{3+} ($^4F_{13/2}$), Sm^{3+} ($^4G_{5/2}$), and Er^{3+} ($^4S_{3/2}$) can be determined by the fittings. Figure 11a shows the changes of the PL emission intensity and lifetimes of Eu^{3+} in YVO_4 films annealed at 500 and 700 °C at different Eu^{3+} doping concentrations. It can be seen that there is a great increase in the PL emission intensity and lifetimes of Eu^{3+} from 500 to 700 °C within all the studied concentrations of Eu^{3+}. The same situation holds for the other three rare earth ions in YVO_4 films annealed from 400 to 800 °C, as listed in Table 1. This is because with the increase of annealing temperature the content of impurities in the film such as −OH, NO_3^-, and CH_2− decreases and the film crystallinity increases. The quenching of the luminescence of the rare earth ions by the vibrations of these impurities decreases, resulting in the increase of their lifetimes and PL emission intensity.

Concentration Effects. By varying the content of the rare earth ions (Eu^{3+}, Dy^{3+}, Sm^{3+}, and Er^{3+}) in YVO_4 films, we determined the compositions with the highest PL emission intensity. Figure 11a−d shows the dependence of the PL emission intensity and lifetimes of the rare earth ion (A) on its doping concentration (x) in $Y_{1-x}VO_4$:xA (A = Eu, Dy, Sm, and Er) films, respectively. It can be found from Figure 11 that the PL emission intensity of Eu^{3+}, Dy^{3+}, Sm^{3+}, and Er^{3+} increases with the increase of their concentrations (x) first, reaching a maximum value at $x = 7$ mol % for Eu^{3+} and at $x = 2$ mol % for Dy^{3+}, Sm^{3+}, and Er^{3+}, respectively, and then decrease with increasing their contents (x) because of the concentration quenching. Thus, the optimum concentration for Eu^{3+} is 7 mol % and those for Dy^{3+}, Sm^{3+}, and Er^{3+} are 2 mol % in YVO_4 films, respectively. Note that the optimum concentration of Eu^{3+} is determined to be 7 mol % in both the 500 and 700 °C annealed samples (Figure 11a), indicating that the optimum concentration is independent of the annealing temperature. Except for Er^{3+}, the optimum concentrations for Eu^{3+}, Dy^{3+}, and Sm^{3+} agree well with those derived from the change of their lifetimes as a function of their doping concentration (x) in YVO_4 films. The lifetimes of Er^{3+} in $Y_{1-x}VO_4$:xEr films decrease monotonically with increasing its concentration (x) in the studied concentration range, although its emission intensity shows a maximum value. A similar situation has been observed before for Er^{3+} in $BaTiO_3$ films.[33] Because the cross-relaxation processes in close Dy^{3+}−Dy^{3+}, Sm^{3+}−Sm^{3+}, and Er^{3+}−Er^{3+} pairs play an important role in their luminescence quenching, their optimum concentrations are much lower than that of Eu^{3+} in the same host lattice, as observed in the current YVO_4 films.[27,33,34] In addition, the typical nonlinear variation of the PL intensity provides further evidence that the film sample consists of doped particles and not of a mixture of AVO_4 (A = Eu, Dy, Sm, and Er) and YVO_4 particles. In the latter case the PL intensity is expected to increase steadily with increasing rare earth ion (A) concentration.[18]

(31) Golab, S.; Ryba-Romanowski, W.; Dominiak-Dzik, G.; Lukasiewicz, T.; Swirkowicz, M. *J. Alloys Compd.* **2001**, *323/324*, 288.
(32) Zhang, H. X.; Kam, C. H.; Zhou, Y.; Han, X. Q.; Buddhudu, S.; Xiang, Q.; Lam, Y. L.; Chan, Y. C. *Appl. Phys. Lett.* **2000**, *77*, 609.
(33) Zhang, H. X.; Kam, C. H.; Zhou, Y.; Han, X. Q.; Xiang, Q.; Buddhudu, S.; Lam, Y. L.; Chan, Y. C. *J. Alloys Compd.* **2000**, *308*, 134.
(34) Lin, J.; Su, Q. *J Mater. Chem.* **1995**, *5*, 1151.

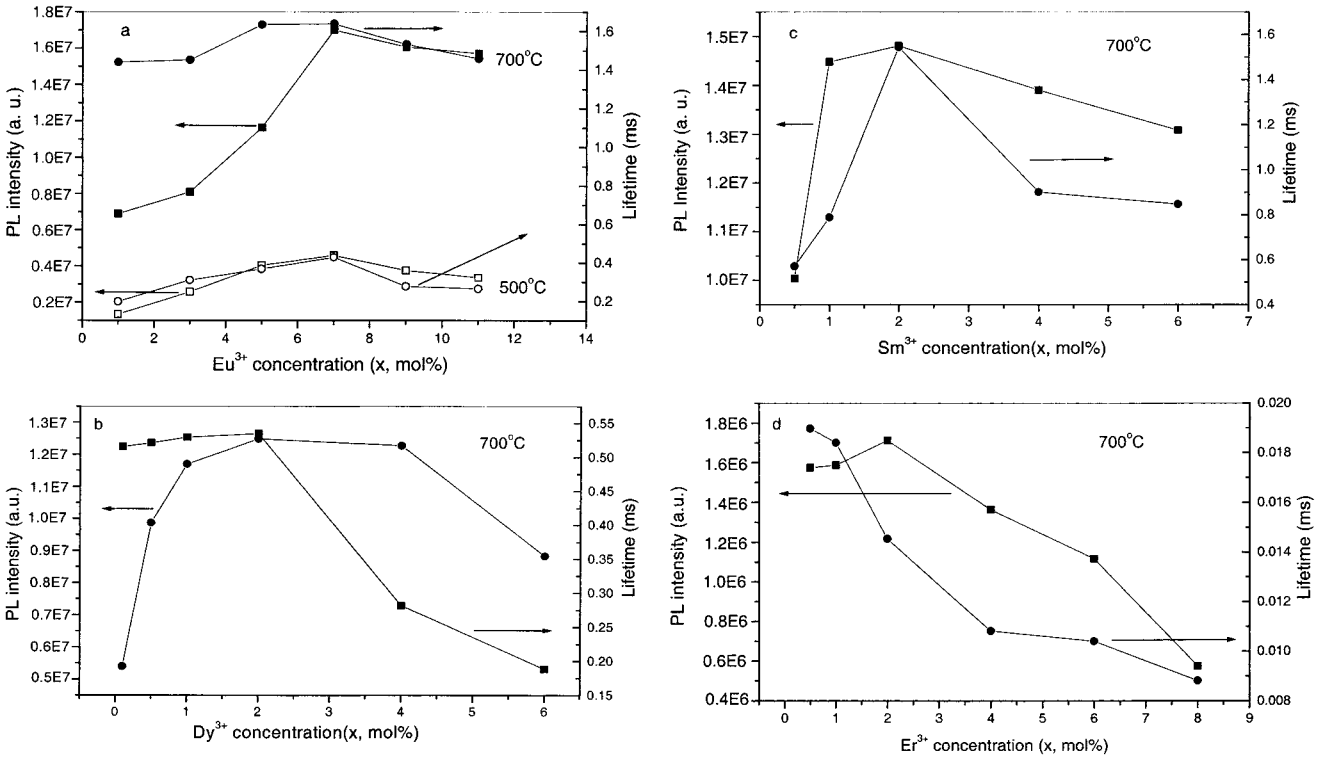

Figure 11. PL emission intensity and lifetimes of A as a function of their concentrations (x) in crystalline $Y_{1-x}VO_4$:xA (A = Eu, Dy, Sm, and Er) films.

Table 1. PL Emission Intensity (I) and Lifetimes (τ) of Dy^{3+}, Sm^{3+}, and Er^{3+} in YVO_4 Films as a Function of Annealing Temperature

		T (°C)				
		400	500	600	700	800
Dy^{3+}	I (a.u.)	1305	1525	7776	22926	41461
	τ (ms)	0.110	0.162	0.217	0.413	0.567
Sm^{3+}	I (a.u.)	406	1228	6496	14977	16375
	τ (ms)	0.066	0.064	0.159	0.931	1.588
Er^{3+}	I (a.u.)	688	1851	11590	34926	50199
	τ (ms)	0.010	0.012	0.013	0.015	0.018

Finally, it should be mentioned that the emission intensity of a layer of the Eu-doped powder is a little higher than that of the film in Figure 1 because of the thickness and particle size difference. With increasing thickness of the film, its emission intensity reaches the same level as that of the powder layer.

IV. Conclusions

Nanocrystalline YVO_4:A (A = Eu^{3+}, Dy^{3+}, Sm^{3+}, and Er^{3+}) phosphor films were successfully prepared by the Pechini sol−gel process using the cheap and nontoxic inorganic compounds as main precursors. These phosphor films can be patterned into ordered bands with different widths (5−60 μm) by the soft lithography technique (micromolding in capillaries). The patterned phosphor film bands present significant shrinkage during the heat treatment process. Upon excitation into the VO_4^{3-} group at 276 nm, the rare earth ions Eu^{3+}, Dy^{3+}, Sm^{3+}, and Er^{3+} show their characteristic red ($^5D_0-^7F_2$), yellow ($^4F_{9/2}-^6H_{13/2}$), orange ($^4G_{5/2}-^6H_{7/2}$), and green ($^4S_{3/2}-^4I_{15/2}$) strong emissions in crystalline YVO_4 phosphor films, respectively, because of an efficient energy transfer from the VO_4^{3-} group to the rare earth ions. The Sm^{3+} and Er^{3+} ions have also shown upconversion luminescence properties in the YVO_4 film host under infrared excitation at 940 and 800 nm, respectively. The current methods can be extended to prepare other various phosphor films and their patterning.

Acknowledgment. This project is financially supported by the foundation of "Bairen Jihua" of Chinese Academy of Sciences, the Outstanding Youth Fund of Jilin Province, Personnel and Educational Ministry of China, Nanometer Center of Changchun Institute of Applied Chemistry, Chinese Academy of Sciences. Dr. Han is also grateful for the financial support of the National Natural Science Foundation of China (50125311).

CM011663Y